energies

MDPI

Article

Pollutant Formation during the Occurrence of Flame Instabilities under Very-Lean Combustion Conditions in a Liquid-Fuel Burner

Maria Grazia De Giorgi [1,*], Stefano Campilongo [1], Antonio Ficarella [1], Gianluigi De Falco [2], Mario Commodo [2] and Andrea D'Anna [3]

1 Department of Engineering for Innovation, University of Salento, 73100 Lecce LE, Italy
stefano.campilongo@unisalento.it (S.C.); antonio.ficarella@unisalento.it (A.F.)
2 Istituto di Ricerche sulla Combustione, CNR, Piazzale Tecchio 80, 80125 Napoli, Italy;
gl.defalco@irc.cnr.it (G.D.F.); commodo@irc.cnr.it (M.C.)
3 Dipartimento di Ingegneria Chimica, dei Materiali e della Produzione Industriale—Università degli Studi di Napoli Federico II, Piazzale Tecchio 80, 80125 Napoli, Italy; anddanna@unina.it
* Correspondence: mariagrazia.degiorgi@unisalento.it; Tel.: +39-0832-297759

Academic Editor: Terese Løvås
Received: 15 December 2016; Accepted: 9 March 2017; Published: 12 March 2017

Abstract: Recent advances in gas turbine combustor design are aimed at achieving low exhaust emissions, hence modern aircraft jet engines are designed with lean-burn combustion systems. In the present work, we report an experimental study on lean combustion in a liquid fuel burner, operated under a non-premixed (single point injection) regime that mimics the combustion in a modern aircraft engine. The flame behavior was investigated in proximity of the blow-out limit by an intensified high rate Charge-Coupled Device (CCD) camera equipped with different optical filters to selectively record single species chemiluminescence emissions (e.g., OH*, CH*). Analogous filters were also used in combination with photomultiplier (PMT) tubes. Furthermore this work investigates well-mixed lean low NO_x combustion where mixing is good and generation of solid carbon particulate emissions should be very low. An analysis of pollutants such as fine particles and gaseous emissions was also performed. Particle number concentrations and size distributions were measured at the exhaust of the combustion chamber by two different particle size measuring instruments: a scanning mobility particle sizer (SMPS) and an Electrical Low Pressure Impactor (ELPI). NO_x concentration measurements were performed by using a cross-flow modulation chemiluminescence detection system; CO concentration emissions were acquired with a Cross-flow modulation Non-dispersive infrared (NDIR) absorption method. All the measurements were completed by diagnostics of the fundamental combustor parameters. The results herein presented show that at very-lean conditions the emissions of both particulate matter and CO was found to increase most likely due to the occurrence of flame instabilities while the NO_x were observed to reduce.

Keywords: lean combustion; flame instability; chemiluminescence emissions; soot

1. Introduction

In recent years technological developments in the aircraft sector has been driven by public awareness and political concern over aviation-induced pollution. Aircraft engine emissions are typically composed of carbon dioxide (CO_2), nitrogen oxides (NO_x), carbon monoxide (CO), smoke and unburned hydrocarbons (UHC).

Lean combustion is actually the main strategy able to satisfy the need of combustors with low NO_x emission as imposed by environmental regulations. Furthermore aircraft gas turbine engines

also emit particulate matter due to incomplete combustion of the fuel, and the conversion of fuel sulfur compounds. At high altitudes, aircraft propulsion systems are the only source of anthropogenic emissions and the exhausted combustion aerosols, may potentially lead to global climate changes. Therefore, great efforts are taken to reduce the emissions of such pollutants.

A reduced operating temperature allows minimizing the emissions of nitrogen oxides [1], but can result in instability in the combustion chamber, compromising the combustor structure and performance [2–4]. In fact under ultra-lean and lean conditions gas turbine burners exhibit flame instability, flashback or lean blowout (LBO), until the flame extinction [5,6].

Dynamic instabilities, also called thermo-acoustic instabilities, are typically due to the interaction of the fluctuating heat release of the combustion process with naturally occurring acoustic resonances, leading to large pressure oscillations within the combustor and mechanical failures [7]. These instabilities have been observed in ground-based lean premixed combustion engines, and should be expected in lean partially premixed or lean direct injection aeroengines. Intermittent bursts of high-amplitude periodic pressure pulsations could be precursors of the onset of these combustion-driven instabilities [8]. Intermittent burst oscillations and large-scale pulsations in the flame have been also observed in combustors close to the lean blowout limit [9,10], with a loss of static flame.

Main flame detachment and reattachment to the flame holder before the complete extinction was observed by Nicholson and Field [10]. Flames transition from stable combustion to LBO through a transient regime manifests itself through large-scale unsteadiness and, most likely, through local variations in heat release [11]. The LBO instability could occur under lean conditions, because the weak combustion is more prone to flame extinction in presence of small perturbations in operating conditions.

If flame extinction appears, generally called a flameout, a highly unfavorable procedure in an aircraft engine is required (engine restart at ground level or even at altitude known as altitude relight). Additionally, in the presence of flame instability, pollutants, as CO and soot, could increase. Hence, to avoid instability, combustors operate with large safety margins, far from instability fuel/air ratio limit, carrying out non-optimal emission performance.

In lean-operated combustors, NO_x and CO emission levels are obtained in a narrow range of fuel-air equivalence ratios and the combustion should be continuously monitored in order to assure the reliable operation in a desired engine operating flight envelope. If the equivalence ratio is too high it leads to high NO_x emissions; on the contrary, if the equivalence ratio is very low it can lead to an unstable combustor operation, resulting in elevated CO emissions, and eventually engine failure.

Hence, the main issue is the optimization of the overall equivalence ratio and the combustor operating parameters to achieve the best combustion performances with a minimum level of NO_x and CO emissions and a wider operating range.

The online monitoring of these phenomena related to combustion instability is an interesting issue of the recent years [12–16]. A good approach is the use of non-intrusive measurements, able to detect the evolution of the optical emissions, such as OH*, CH*, or CO_2* radical species. The trends of these species can be considered as a marker of the combustion status as well as of LBO limit [17,18]. A high acquisition rate is crucial to analyze the dynamic phenomena typical of the lean flame [19–22].

In the current literature it is known that the OH* and CH* peaks decrease in intensity when going from a rich flame to a leaner flame [23]. However only a few studies have investigated flame blowout in presence of a lean liquid fueled combustor [19,24–26], which is characterized by unique processes such as atomization and evaporation not involved in gas combustion.

Yi and Santavicca [19] investigated both the flame structure and the combustion instability characteristics in a turbulent liquid-fueled swirl-stabilized lean direct fuel injection combustor. The imaging of CH* chemiluminescence measurements showed that during combustion instability there are mainly variations in the chemiluminescence intensity rather than in the spatial distribution of heat release.

The present paper aims to cover up the lack of a deep understanding of the effect of fuel/air ratio values, close to lean blowout, on combustion stability of liquid fuels, by analyzing both optical emissions and pollutants.

Hence this study investigates combustion performance and static stability margin in a non-premixed liquid-fueled lean burn combustor near the LBO limit. Flame stability sensing is primarily based on detecting LBO precursor events in the flame optical emission signals. The chemiluminescence emissions in the Ultraviolet (UV) spectral range were acquired by a high rate CCD camera equipped with an intensifier and by a photomultiplier tube (PMT), using different optical filters. This permitted us to characterize the flame stability.

The exhaust gaseous and particle emissions were also analyzed near the LBO limit in order to relate the occurrence of combustion instability with the main pollutants trends. For the particle emissions, a scanning mobility particle sizer (SMPS) and the electrical low-pressure impactor (ELPI) were used to measure particle size distributions. To the best of our knowledge, this is the first attempt to measure combustion aerosol emissions in gas turbine burners near the lean blowout combustion conditions.

2. Experimental Set-Up

2.1. Combustor Facility and Flame Conditions

A liquid-fueled gas-turbine derived combustor (modified for laboratory investigations with a thermal power of 300 kW) was used for experimental purposes; the burner [27,28], shown in Figure 1, is located at the Green Engine Laboratory of the University of Salento (Lecce, Italy). The cylindrical combustion chamber has an axial dimension of 29 cm and a diameter of 14 cm. Figure 2a shows a schematic view of all the components and the instrumentations involved in the setup.

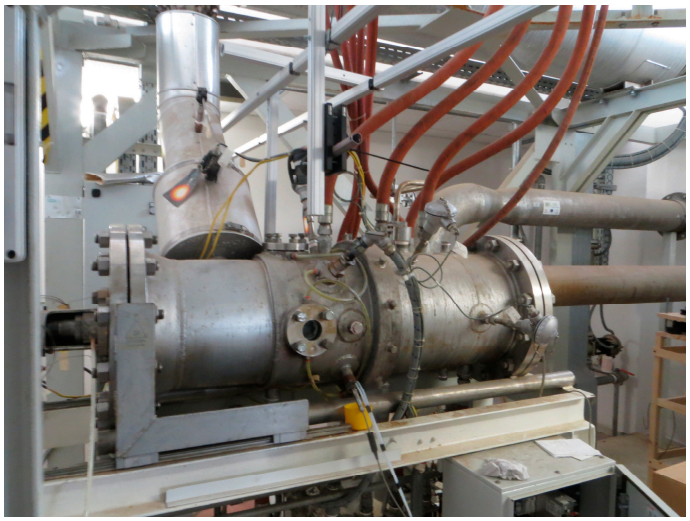

Figure 1. The green engine burner.

The total air flow rate was fixed at 85 $\times$ 10^{-3} kg/s with a ratio of 1:11 between primary and secondary air flow, respectively. The air passage consists of two concentric annular tubes. The inner one is equipped with eight-septa, 45° swirler. At the exit, the combustion chamber contracts to a cylindrical exhaust gas nozzle.

The burner can operate both in non-premixed (single injection) and partially-premixed (multipoint injection) fueling modes. In this work the non-premixed mode has been investigated; the inherent flow path is depicted in Figure 2b. The fuel (diesel oil) is driven in a single-hole injector and enters in the chamber along the longitudinal axis. The injector hole has a diameter of 0.5 mm and a spray angle of 45°.

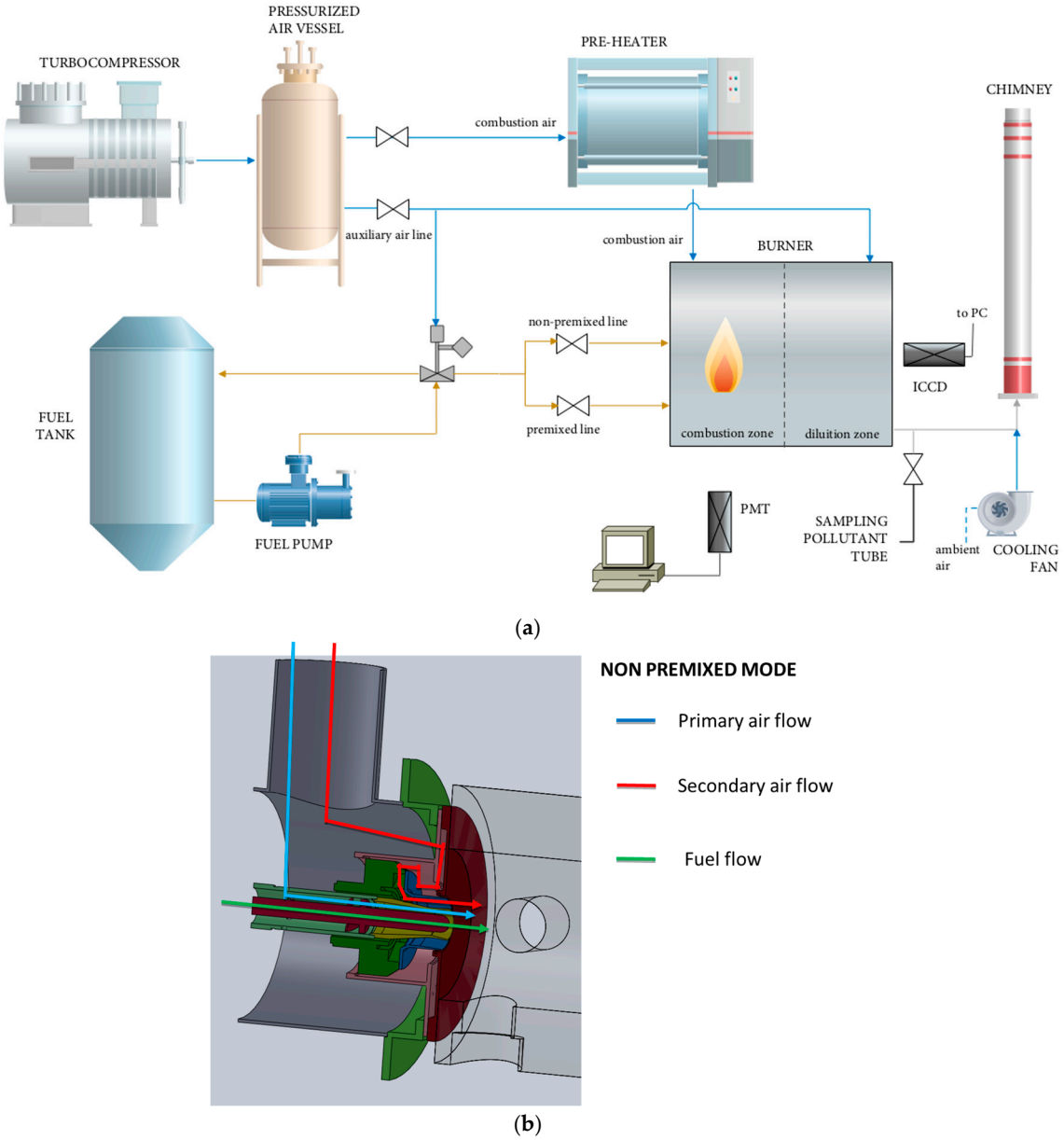

Figure 2. (**a**) Schematic view of the experimental apparatus; and (**b**) flow path in the non premixed configuration.

The air was preheated at 500 K, keeping the pressure in the chamber (without combustion) constant at 1 bar. To investigate the effect of the instability condition, the measurements have been performed by changing the equivalence ratio, Φ, defined as:

$$\Phi = \frac{\left(\frac{m_{fuel}}{m}_{air}\right)}{\left(\frac{m_{fuel}}{m}_{air}\right)_{stoichiometric}} \quad (1)$$

Lean blowout conditions were reached mainly by lowering the fuel flow rate, while the air flow rate was approximately constant.

In detail the exhaust emissions were acquired for several operating conditions in the range Φ = 0.12–0.51. The imaging post processing technique and the detailed analysis of the data from the optical tools were applied to the cases where the flame is defined as very-lean, which means Φ was

very low (as reported in Table 1), near the lean blowout limit, which is at $\Phi = 0.12$. Each variation of the fuel/air equivalent ratio was maintained for 10 min, to ensure both stabilization of the equivalence ratio around the target value and steady state thermal boundary conditions.

Table 1. Test conditions.

Case	Air (g/s)	Fuel (g/s)	Φ
I	83.92	1.81	0.348
II	84.23	1.54	0.266
III	86.10	1.30	0.220

2.2. Chemiluminescence Data Acquisition and Processing

The combustor is equipped with circular optical accesses with a diameter of 50 mm: three circumferential and one frontal windows. Each window has two quartz glass plates stacked together with a small gap in between. The inner glasses are exposed to the flames. Within the gap, an air mass flow is guided accomplishing a convective window cooling.

A MEMRECAM GX-3® (NAC Image Technology, Simi Valley, CA, USA) high speed CCD camera [29], was located perpendicularly to the flame axis to permit a suitable flame view. Hereafter, visible-range images from the circumferential windows were acquired with a resolution of 288 pixels × 368 pixels and a frequency of 10 kHz; time duration was 1 s. A suitable flame view area of 67 mm and 50 mm was recorded during the acquisitions. The camera is also equipped with the automatic function of "black balance" that corrects the black level sensor and erases noise elements.

OH* and CH* chemiluminescence line-of-sight measurements were acquired from the circumferential window by using two Photo Multiplier Tube Single Stage (PMTSS) photomultiplier tubes from Thorlabs® (Munich, Germany) [30] without optical lens and coupled through a beam splitter equipped with two interference filters with central wavelength of 307 nm and 431 nm respectively, with a full width at half maximum (FWHM) of 10 nm. The signals were recorded by a NI-USB 6008 data acquisition (DAQ) device of National Instruments® (Austin, TX, USA) [31] with an acquisition frequency of 5 kHz and 1 s of acquisition time for each test.

The chemiluminescence emissions were also acquired from the frontal window using the a Phantom Miro M320S® (Vision Research Inc., Wayne, NJ, USA) high-speed digital camera [32], with a maximum frame rate at full resolution (1920 × 1080) of 1540 Hz, a sensitivity of 1100 ISO and a pixel depth of 12 bit. The camera was equipped with an intensifier by Lambert Instrumentation® (Groningen, The Netherlands) [33]; the intensifier has a S20 (UV) photocathode material, P46 phosphor screen and a 270–450 nm spectral range for max response. The intensifier gain was set to 250 for the CH* and 600 for the OH* emissions. The quantum efficiency (QE) of the intensifier/CCD coupling for the two wavelength is about 0.6% for OH* and 3.85% for the CH*.

The images for the analysis were taken with a resolution of 651 pixels × 407 pixels, a frequency of 1 kHz and a flame view area of 59 mm and 36.8 mm. The mean values of the PMT signals were calculated using the raw signals. On the contrary the variance was evaluated starting from the signal normalized with respect to the averaged value.

The images were processed using MATLAB® (MathWorks®, Natick, MA, USA) with user-developed routines. The signal of each image was represented through an intensity value, codified using 8 bits, ranging from 0 ("black" correspondent to ultra-low luminosity) to 255 ("white" corresponds to ultra-high luminous). In order to avoid taking into account the light from reflections at the boundaries of the circular window a crop processing of the images was defined, with an appropriate quasi-circular mask.

For the evaluation of the mean value and the variance associated with the data from the camera, the original signal was normalized with respect to the space and the time (or better, with respect to the number of time-step in which an image is taken), as follows:

$$I_N(x,y,t) = \frac{I(x,y,t) \cdot L \cdot M \cdot N}{\sum_{t=1}^{L} \sum_{x=1}^{N} \sum_{y=1}^{M} I(x,y,t)} \quad (2)$$

where M is the number of pixels in the x direction, N was the number of pixels in the y direction of each image and L was the number of acquired images for each condition. In the present acquisition, M was equal to 651, N to 407 pixels and L was 1000.

2.3. Gaseous Emissions Measurements

Gaseous emissions were acquired through a complete analyzer system (PG-350E Horiba, Leichlingen, Germany) equipped with gas sampling, sample conditioning, analyzer and system control units. The NO_x detector uses the cross-flow modulation chemiluminescence detection system; the SO_2 and CO detectors operate with a cross-flow modulation, non-dispersive infrared (NDIR) absorption method; the CO_2 unit uses the standard non-dispersive infrared (NDIR) absorption method; and the O_2 unit uses the paramagnetic method. The gas analyzer recorded the gas value every 1 s. The measurement uncertainties of NO_x, CO, O_2 and CO_2 were less than $\pm 1\%$. The measurement sensitivities were 1 ppm for NO_x, CO and O_2 emissions and 0.01% for CO_2 emission.

2.4. Particle Size Measurements: DMA SYSTEM and ELPI System

Particle size distributions at the exhaust of the combustion chamber were measured by using two different commercially available instruments: a scanning mobility particle sizer (SMPS, TSI Model 3938, TSI, Shoreview, MN, USA) and an Electrical Low Pressure Impactor (ELPI, Dekati Ltd., Kansagala, Finland). These two systems were employed to acquire particle size distributions within a size range from 2.5 nm to 10 µm. For the SMPS measurements, sampled particles were first charged by means of a X-ray neutralizer (TSI Model 3088), later selected through a nanoDMA (TSI Model 3085, TSI, Shoreview, MN, USA), and finally counted by means of an Ultrafine Condensation Particle Counter (UCPC, TSI Model 3776, TSI, Shoreview, MN, USA) that allows counting particles as small as 2.5 nm. This measuring technique is based on the differential mobility analysis (DMA), which furnishes the possibility of determining the size distribution of particles at the exhaust of a generic combustor by scanning the particle electrical mobility, Z, in a variable electric field [34].

Particle size distributions were also measured using the ELPI measurement system. The ELPI is a particle size spectrometer for real-time monitoring of aerosol particle size distributions [35]. The instrument is composed by a corona charger, a 12-stage cascade low-pressure impactor and a multichannel electrometer, which allows covering the entire measurement size range from 30 nm to 10 µm. An extra filter stage was added in order to extent the measurement size range down to 7 nm. The charged particles are collected on the 13 collection plates, and the current value of each channel, which is proportional to the number of particles collected, is converted into particle aerodynamic size distribution using relationships describing particle size dependent properties of the charger and the impactor stages [36]. The instrument sample flow is 10 L/min. Measurement data were then processed by the ELPI XLS4.05 software (Dekati Ltd.). An overall dilution ratio of 5 was used for both measurements. This value is above the critical dilution ratio to prevent particles form coagulation as reported elsewhere [37].

3. Experimental Results and Discussion

3.1. Flame Characterization and Instability Detection by Chemiluminescence

Flame instabilities could be related to blow out, flashback, and resonance established through the interaction of acoustic waves and combustion. In the present study, the flame instabilities in conditions close to lean blowout have been investigated by the analysis of chemiluminescence measurements. In order to evaluate the flame regime and the occurrence of flame instabilities the temporal chemiluminescence data acquired by PMT and by the high speed CCD camera were analyzed.

In Figure 3 the images recorded through the visible CCD camera in broadband configuration are shown at different time instants and for different values of the fuel/air ratio. For high fuel /air equivalence ratio values there is always a well-defined combustion area and the flame looks stable and compact. With the decreasing of the fuel the flame moves farther downstream from the combustor inlet, becoming less uniform in the space and less intense in the luminosity. This effect is due to the fuel/air ratio reduction below the flammability limits, causing the local quenching of the flame.

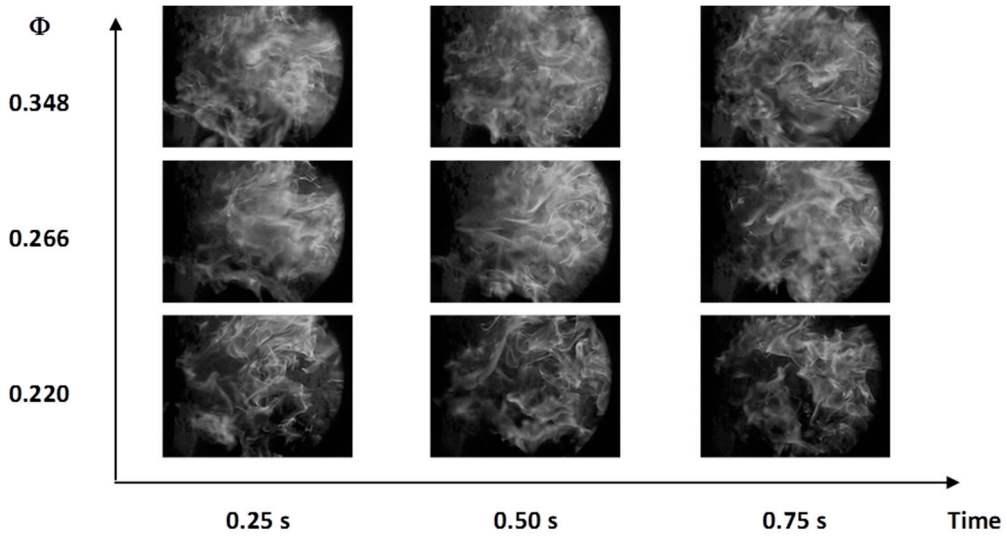

Figure 3. Temporal variation of chemiluminescence intensity in the visible spectral range for different Φ; the images were acquired with MEMRECAM in broadband configuration.

The transient signals of CH* and OH* chemiluminescence emissions, which were acquired by the PMTs equipped with interference filters, have been analyzed. Figure 4 shows the signals for the three operating conditions; the intensity diminishes with increasing amount of fuel and the fluctuation level of unstable flame close to blowout (Case III) is found to be higher as compared to the stable flame case (Case I).

The enhanced fluctuation level of unstable flame can be attributed to the random local flame extinction and re-ignition. Besides this, local extinction leads to a very low CH* chemiluminescence signal intensity. In Table 2, OH* and CH* (evaluated taking into account the QE correction) mean and variance values were compared for different test conditions. From the statistical analysis of CH* chemiluminescence signals, it is evident that the mean CH* intensity and the variance, decrease and increase respectively as the blowout is approached.

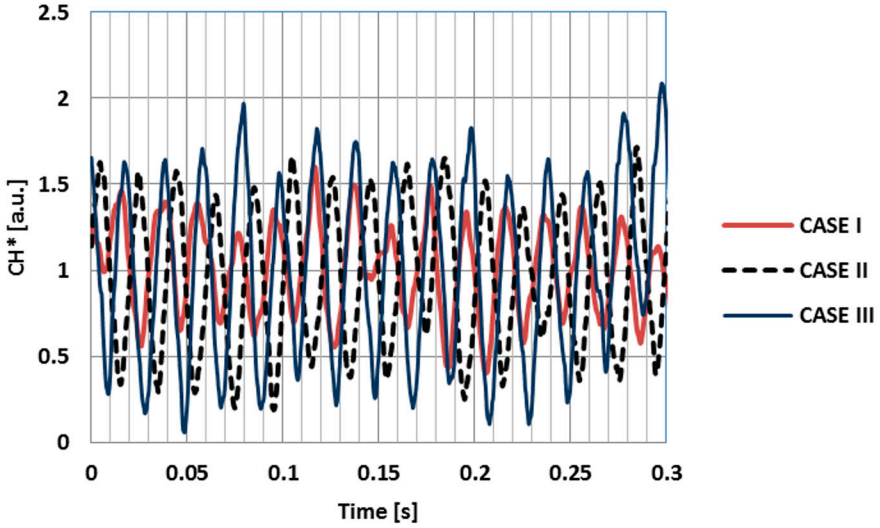

Figure 4. Temporal variation of CH* chemiluminescence intensity from PMT for different Φ.

Table 2. Mean values and variance of the OH* and CH* chemiluminescence signals acquired by PMT.

Case	OH* Mean Value	OH* Variance	CH* Mean Value	CH* Variance	CH*/OH* Mean Value
I	4.903	0.050	23.300	0.065	4.752
II	5.008	0.049	14.810	0.161	2.957
III	4.463	0.062	12.175	0.256	2.728

In particular a high variability of the CH* signals moving from stable to unstable conditions may be observed, as the CH* variance in the leanest condition (Case III) is four times higher than the one at richer mixture (higher fuel-air ratio) and more stable combustion (Case I).

While the CH* mean value for the Case III is approximately half of the value for the Case I. Even if the same trend is evident for the OH* emissions the rise of the variance and the decrease of the mean value towards the leanest condition is not so significant, i.e., the variance changes from 0.05 to 0.062.

It appears interesting to take into consideration as the CH*/OH* ratio, which is related to the flame's global heat release [38], decreases of 30% lowering the fuel/air equivalence ratio from 0.35 to 0.22.

The variance/mean intensity ratio is plotted in Figure 5 for both the CH* and OH* emissions. Physically the variance/mean intensity ratio takes into account the effect of both reduction in heat release rate and rise in the frequency of random local extinction and reignition events occurring in the flame near the blowout. The rise of this ratio at low fuel/air ratio is more evident for the CH* signals, in fact the ratio at leanest conditions (Case III) is six time the value at richest mixture (Case I). Moreover considering the OH* emission, the increase of this ratio is low, thus indicating that the CH* signal is more suitable to identify unstable flame approaching the blowout.

Figures 6 and 7 show the mean value and variance maps of the data acquired by the intensified camera from the frontal optical window. On these maps, the longitudinal axis of the combustion chamber was taken as reference and its position corresponds to the coordinates (0, 0) in the images. The other coordinates are reported as distance from the axis in mm. The protrusion, visible in the Intensified Charge-Coupled Camera (ICCD) map, is a thermocouple. The OH* and CH* intensity distributions are qualitatively quite similar, with a strong concentration on the peripheral region.

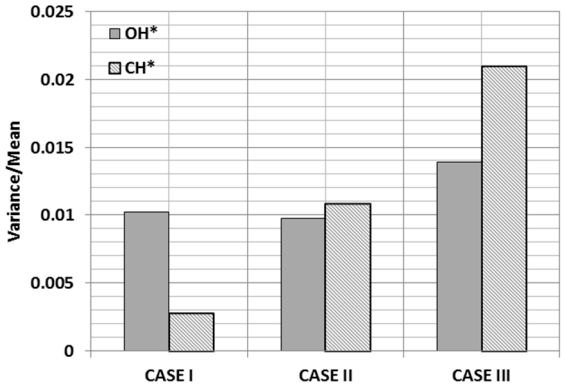

Figure 5. Variance/mean ratio for the intensity of CH* and OH* chemiluminescence signals from PMT.

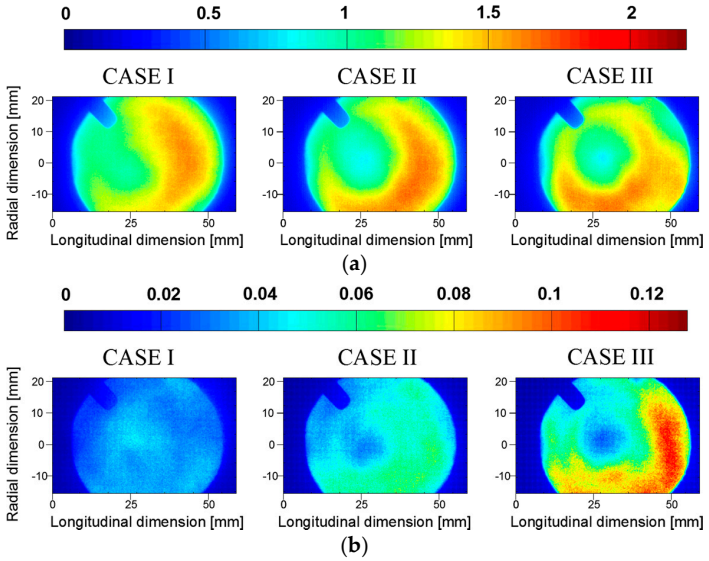

Figure 6. OH* chemiluminescence emissions maps acquired with the ICCD camera: (**a**) mean value and (**b**) variance.

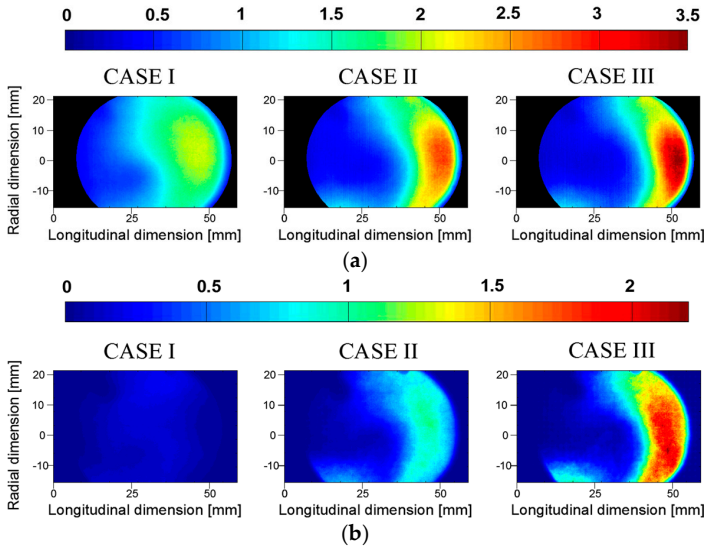

Figure 7. CH* chemiluminescence emissions maps acquired with the ICCD camera: (**a**) mean value and (**b**) variance.

The map of the mean values of OH* emissions (Figure 6a) doesn't show relevant changes in the three analyzed conditions and the results are not useful for the detection of blowout onset. Moreover the variance for both the emissions shows a more marked rise moving to leaner conditions. In Figure 6b the OH* maximum variance rises from 0.05 to 0.12.

Figure 7 confirms the high variability of the chemiluminescence signal also for the CH* emission, in terms of both the mean value and the variance, in accordance with the acquisition by the PMT. As for the PMT measurements, the imaging acquisitions confirm that the increase of the CH* variance is higher with respect to the OH* emissions. In Figure 7b the maximum variance in the case III is approximately two times the value at the highest fuel/air ratio.

3.2. Analysis of the Exhaust Gas Emissions

In Figure 8 the combustion chamber temperature and exhaust pollutants (nitrogen oxide and carbon monoxide) are reported at different fuel/air equivalent ratios Φ. The thermocouple used for the measurements is located in the proximity of the burner outlet, very close to the sampling tube for pollutant, located just after the burner exit. The temperature (Figure 8a) presents an approximately linear trend with the increasing of the fuel flow rate.

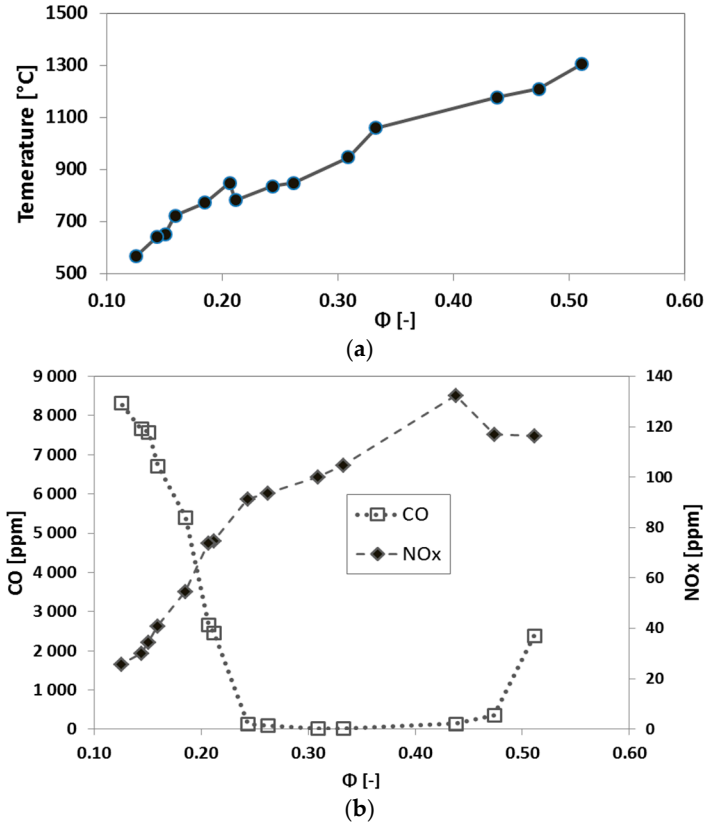

Figure 8. (**a**) Combustion chamber temperature and (**b**) CO and NO_x emissions as function of the equivalent fuel/air ratio variance.

The blowout behavior could be detected by means of emissions analysis (Figure 8b), and in particular of CO measurements. Gas emissions measurements confirm the main conclusions of the flame imaging analysis in terms of fuel/air ratio at which LBO occurs.

Approaching the LBO condition, the residence time is not long enough for the whole oxidation of CO due to the low flame temperature, hence, for low values of Φ the CO emissions abruptly increase in proximity of the lean blowout limit that occurs at about Φ = 0.25. At these very-lean conditions, NO_x emissions are reduced up to 80% with respect to the condition at Φ equals to about 0.5.

Figure 9 shows the trend of all the species detectable with the PG-350E Horiba for Case I and Case III. The NO_x emissions decreases from 54 (Case I) to 28 ppm (Case III) while CO rises from 10 to 32 ppm. At the same time O_2 slightly increases and CO_2 diminishes.

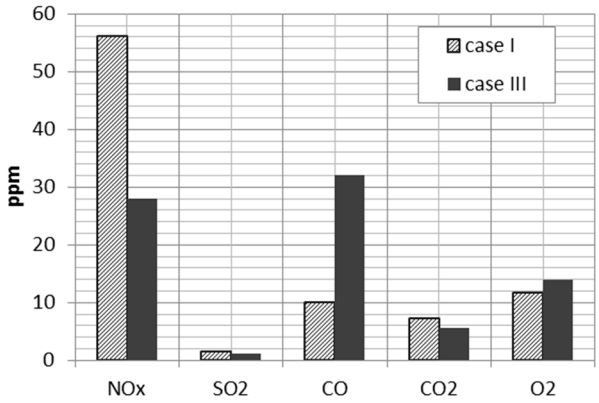

Figure 9. Emissions at two fuel/air ratio close to LBO.

3.3. Particle Concentrations and Number Size Distributions

Figure 10 reports the particle size distributions, PSDs, measured at the exhaust of the combustion chamber using both a SMPS and an ELPI system for two selected test conditions: Case I and Case III, i.e., across the LBO condition. Data were corrected for the employed dilution ratio. For both combustion conditions, the PSDs present a clear bimodal shape with a first mode of particles, commonly referred to as nucleation mode, characterized by particles whose size is lower than 10 nm, and a second mode, the accumulation mode, composed by larger particles mainly centered in the size range 50–500 nm. By comparing the PSDs for the two test conditions it shows a rather invariance of the position of the first mode of particles while the second mode results shifted towards larger particles when changing the combustion regime to the leaner condition, i.e., from Case I to Case III.

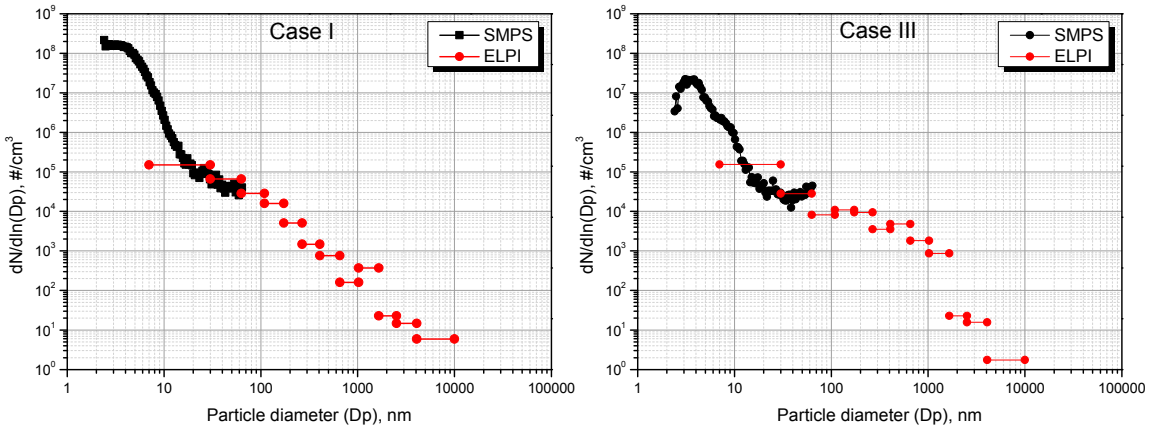

Figure 10. Particle size distributions measured by SMPS and ELPI at the exhaust of the combustor for two selected equivalence ratios.

It is worth mentioning that a bimodal shape of the particle size distribution, similar to the one reported herein, has been already observed by measuring ultrafine particles from a gas-turbine burning several hydrocarbon and bio-derived liquid fuels [37]. In addition, the presence of a bimodal particle size distribution has been observed under diesel [39] and gasoline spark ignition engine operations [40], although for the gasoline engine particle number emission above the background level was mainly

reported to occur during specific combustion regimes such as during acceleration, high-speed cruise, and during cold–cold starts [39].

Within the engine community, the origin of the nucleation mode, i.e., whether it is formed by semivolatile particles, mainly composed of sulfuric acid and heavy hydrocarbons, or by solid particles produced during the combustion process, is subject to debate [36]. Kittelson et al. [39] investigating both on-road and laboratory aerosol emission from four, heavy-duty diesel truck engines showed that nuclei mode particles mainly consisted of heavy hydrocarbons. The authors found that the most of the volume of the nuclei particles disappeared after heating to 400 °C, together with a volatility behavior similar to that of C_{24}–C_{32} *n*-alkanes suggesting a significant contribution of the nuclei particles from lubricating oil. De Filippo and Mariq [41], however, reports evidence of a "solid" particle nucleation mode that accompanies normal soot emissions in a study of aerosol emissions from two light-duty diesel vehicles operated with ultralow sulfur fuel. More recently, nonvolatile nanoparticle emissions have been also reported to occur in a heavy-duty engine running alternative diesel fuels [42]. The presence of a "solid" nuclei particles formed during combustion, with particle size of the order of few nanometers and distinct from soot particles, is also consistent to what has been found by in-situ and ex-situ analysis of carbon nanoparticles formation and evolution in laboratory premixed and diffusion flames [43–47].

The accumulation mode ranges in size from about 50–500 nm, in this mode, carbonaceous particles grew up through the condensation of hydrocarbons or agglomeration with other particles. Overall an increase in the total particle volume fraction of the measured combustion aerosol when changing the combustion regime from the lean (Case I) to the very-lean condition (Case III) can be observed. Indeed, from the measured PSD shown in Figure 10, particle volume fractions have been calculated. These resulted to be 9.24×10^{-9} cm^3/cm^3 for the Case I and 1.45×10^{-8} cm^3/cm^3 for the Case III condition. The observed increase of the particle volume fraction from Case I to Case III is in agreement to the gas phase composition analysis showing an overall increase in the concentration of CO for the same test conditions. Hence, pollutants characterization underlines that very-lean combustion, in proximity of the blowout limit, reduces NO_x to a great extent but deteriorates pollutants, such as soot particles and CO.

It should be noted that our results only refer to the investigated non-premixed (single injection) conditions. Partially-premixed (multipoint injection) fueling modes are not covered in the present study. Therefore, future works is needed to assess whether or not the formation of nucleation mode particles may be relevant also in other combustion, e.g., fuel/air mixing, configurations.

4. Conclusions

In this study research on the combustion dynamic characteristics of a lean liquid fuel burner, operated in non-premixed (single point injection) regime, was carried out. The study was performed under different fuel/air ratio values and the combustion performance was compared.

The results suggest that the optimization of operation settings, in terms of fuel/air ratio, in single injection mode should be a compromise of values that reduce gaseous and particle emissions without affecting flame stability. In particular lowering the equivalence ratio at values smaller than 0.26, in proximity of the blow-out limit, showed a significant reduction of NO_x but also a rapid increase of static combustion instabilities, soot particle and CO emissions. Furthermore, the techniques implemented herein are suitable to reveal the occurrence of combustion instabilities, thus avoiding the operation of combustors with too large safety margins, far from instability fuel/air ratio boundaries, but corresponding to non-optimal emission performance.

Chemiluminescence data were acquired to characterize the flame structures and dynamics at stable and near-lean blowout (LBO) conditions. In particular the OH*, CH* and CO_2* chemiluminescence emissions of the flame were recorded by a high-speed camera and photomultiplier tubes, equipped with different optical filters, were used. CH* chemiluminescence signals present a decrease of the mean intensity and an increase of the variance as the blowout is approached. This trend is not so

remarkable in the case of OH* emissions. Then the CH* variance/mean intensity ratio, which takes into account the effect of both reduction in heat release rate and rise in the frequency of random local extinction and reignition events, increases at low fuel/air ratio.

In proximity of the blow-out limit, pollutant measurements underline that very-lean combustion reduces NO_x to a great extent, but deteriorates levels of pollutants such as soot and CO. The particle size distributions present a clear bimodal shape with a first mode of particles, commonly referred to as nucleation mode, characterized by particles whose size is lower than 10 nm, and a second mode, the accumulation mode, composed by larger particles mainly centered in the 50–500 nm size range. The second mode results shifted towards larger diameters approaching the leaner condition. Furthermore, an increase of the particle volume fraction was evident when changing the combustion regime from the lean to the very-lean condition, in agreement to the gas phase composition analysis showing an overall increase in the concentration of CO for the same test conditions.

Acknowledgments: We thank Andrea Riso for his powerful help during experiments. We also thank the reviewers for their precious suggestions.

Author Contributions: All the authors have co-operated for the preparation of the work. Maria Grazia De Giorgi and Antonio Ficarella conceived and designed the experiments; Maria Grazia De Giorgi, and Stefano Campilongo performed the experiments and analyzed the data regarding the flame characterization by CCD camera and PMT. Gianluigi De Falco, Mario Commodo, and Andrea D'Anna performed the acquisitions and the analysis of the exhaust emissions.

Conflicts of Interest: The authors declare no conflict of interest.

References

1. Lazik, W.; Doerr, T.; Bake, S.; Bank, R.; Rackwitz, L. Development of lean-burn low-NO_x combustion technology at rolls-royce deutschland. In Proceedings of the ASME Turbo Expo 2008: Power for Land, Sea, and Air, Berlin, Germany, 9–13 June 2008; Volume 3, pp. 797–807.
2. Schildmacher, K.U.; Koch, R.; Bauer, H.J. Experimental characterization of premixed flame instabilities of a model gas turbine burner. *Flow Turbul. Combust.* **2006**, *76*, 177–197. [CrossRef]
3. Matalon, M. Intrinsic flame instabilities in premixed and nonpremixed combustion. *Annu. Rev. Fluid Mech.* **2007**, *39*, 163–191. [CrossRef]
4. Campa, G.; Camporeale, S.M. Prediction of the thermoacoustic combustion instabilities in practical annular combustors. *J. Eng. Gas Turbines Power* **2014**, *136*, 091504. [CrossRef]
5. Füri, M.; Papas, P.; Monkewitz, P.A. Non-premixed jet flame pulsations near extinction. *Proc. Combust. Inst.* **2000**, *28*, 831–837. [CrossRef]
6. Rosentsvit, L.; Levy, Y.; Erenburg, V.; Sherbaum, V.; Ovcharenko, V.; Chudnovsky, B.; Herszage, A.; Talanker, A. Extension of the combustion stability range in dry low NO_x lean premixed gas turbine combustor using a fuel rich annular pilot burner. *J. Eng. Gas Turbines Power* **2014**, *136*, 051509. [CrossRef]
7. Lieuwen, T.C.; Yang, V. (Eds.) *Combustion Instabilities in Gas Turbine Engines: Operational Experience, Fundamental Mechanisms, and Modeling*; American Institute of Aeronautics and Astronautics (AIAA): Washington, DC, USA, 2006.
8. Kabiraj, L.; Sujith, R.I. Nonlinear self-excited thermoacoustic oscillations: Intermittency and flame blowout. *J. Fluid Mech.* **2012**, *713*, 376–397. [CrossRef]
9. Nair, V.; Sujith, R.I. Intermittency as a transition state in combustor dynamics: An explanation for flame dynamics near lean blowout. *Combust. Sci. Technol.* **2015**, *187*, 1821–1835. [CrossRef]
10. Nicholson, H.; Field, J. Some Experimental techniques for the investigation of mechanism of flame stabilization in the wakes of bluff bodies. *Symp. Combust. Flame Explos. Phenom.* **1948**, *3*, 44–68. [CrossRef]
11. Muruganandam, T.M.; Nair, S.; Scarborough, D.; Neumeier, Y.; Jagoda, J.; Lieuwen, T.; Seitzman, J.; Zinn, B. Active control of lean blowout for turbine engine combustors. *J. Propuls. Power* **2005**, *21*, 807–814. [CrossRef]
12. Ballester, J.; Sanz, A.; González, M.A. Investigation of the characteristics and stability of air-staged flames. *Exp. Therm. Fluid Sci.* **2008**, *32*, 776–790. [CrossRef]
13. Hernández, R.; Ballester, J. Flame imaging as a diagnostic tool for industrial combustion. *Combust. Flame* **2008**, *155*, 509–528. [CrossRef]

14. Töreyin, B.U.; Dedeoglu, Y.; Güdükbay, U.; Cetin, A.E. Computer vision based method for real-time fire and flame detection. *Pattern Recognit. Lett.* **2006**, *27*, 49–58. [CrossRef]
15. Tuntrakoon, A.; Kuntanapreeda, S. *Image-Based Flame Control of a Premixed Gas Burner Using Fuzzy Logics*; Lecture Notes in Computer Science; Springer: Berlin/Heidelberg, Germany, 2003; Volume 2871, pp. 673–677.
16. Sun, D.; Lu, G.; Zhou, H.; Yan, Y. Condition monitoring of combustion processes through flame imaging and kernel principal component analysis. *Combust. Sci. Technol.* **2013**, *185*, 1400–1413. [CrossRef]
17. Ballester, J.; García-Armingol, T. Diagnostic techniques for the monitoring and control of practical flames. *Prog. Energy Combust. Sci.* **2010**, *36*, 375–411. [CrossRef]
18. Ballester, J.; Hernández, R.; Sanz, A.; Smolarz, A.; Barroso, J.; Pina, A. Chemiluminescence monitoring in premixed flames of natural gas and its blends with hydrogen. *Proc. Combust. Inst.* **2009**, *32*, 2983–2991. [CrossRef]
19. Yi, T.; Santavicca, D.A. Flame spectra of a turbulent liquid-fueled swirl-stabilized lean-direct injection combustor. *J. Propuls. Power* **2009**, *25*, 1058–1067. [CrossRef]
20. Keshav, S.; Utkin, Y.G.; Nishihara, M.; Rich, J.W.; Adamovich, I.V.; Bao, A. Studies of chemi-ionization and chemiluminescence in supersonic flows of combustion products. *J. Thermophys. Heat Transf.* **2008**, *22*, 157–167. [CrossRef]
21. Allouis, C.; Pagliara, R.; Saponaro, A. Fast infrared imaging for combustion stability analysis of industrial burners. *Exp. Therm. Fluid Sci.* **2012**, *43*, 2–8. [CrossRef]
22. Allouis, C.; Beretta, F.; Ferrante, A.; Saponaro, A. Fast Infrared Imaging To Study Industrial Burner Combustion. In Proceedings of the 2009 European Combustion Meeting, Istanbul, Turkey, 5–9 July 2009.
23. Smith, G.P.; Luque, J.; Park, C.; Jeffries, J.B.; Crosley, D.R. Low pressure flame determinations of rate constants for OH(A) and CH(A) chemiluminescence. *Combust. Flame* **2002**, *131*, 59–69. [CrossRef]
24. De Giorgi, M.G.; Sciolti, A.; Campilongo, S.; Ficarella, A. Assessment of the combustion behavior of a pilot-scale gas turbine burner using image processing. In Proceedings of the ASME 2014 Power Conference, Baltimore, MA, USA, 28–31 July 2014.
25. De Giorgi, M.G.; Sciolti, A.; Pescini, E.; Ficarella, A. Frequency analysis and predictive identification of flame stability by image processing. In Proceedings of the 8th International Conference on Energy Sustainability Sustainable Collocated with the ASME 2014 12th International Conference on Fuel Cell Science, Engineering and Technology, Boston, MA, USA, 30 June–2 July 2014.
26. Ruao, M.; Costa, M.; Carvalho, M. A NO_x diagnostic system based on a spectral ultraviolet/visible imaging device. *Fuel* **1999**, *78*, 1283–1292. [CrossRef]
27. De Giorgi, M.G.; Sciolti, A.; Campilongo, S.; Ficarella, A. Image processing for the characterization of flame stability in a non-premixed liquid fuel burner near lean blowout. *Aerosp. Sci. Technol.* **2016**, *49*, 41–51. [CrossRef]
28. De Giorgi, M.G.; Sciolti, A.; Campilongo, S.; Ficarella, A. Experimental data regarding the characterization of the flame behavior near lean blowout in a non-premixed liquid fuel burner. *Data Brief* **2016**, *6*, 189–193. [CrossRef] [PubMed]
29. Memrecam®. User's Manual. Available online: http://www.nacinc.com/products/memrecam-high-speeddigital-cameras/gx-3 (accessed on 15 July 2016).
30. Thorlabs Amplified Photomultiplier User Manual. Available online: http://www.thorlabs.de/thorcat/17400/PMM01-Manual.pdf (accessed on 15 July 2016).
31. National Instruments Data Acquisition (DAQ) Device NI-USB6008 Specifications. Available online: http://www.ni.com/datasheet/pdf/en/ds-218 (accessed on 15 July 2016).
32. Phantom Micro M320 High-Speed Digital Camera. Available online: https://www.abelcine.com/store/Phantom-Miro-M320S-High-Speed-Digital-Camera/ (accessed on 15 July 2016).
33. High-Speed Intensified Camera Attachment. Available online: http://www.lambertinstruments.com/hicatt (accessed on 15 July 2016).
34. De la Mora, J.F.; de Juan, L.; Eichler, T.; Rosell, J. Differential mobility analysis of molecular ions and nanometer particles. *TrAC Trends Anal. Chem.* **1998**, *17*, 328–339. [CrossRef]
35. Marjamäki, M.; Keskinen, J.; Chen, D.R.; Pui, D.Y.H. Performance evaluation of the electrical low-pressure impactor (ELPI). *J. Aerosol Sci.* **2000**, *31*, 249–261. [CrossRef]
36. Keskinen, J.; Pietarinen, K.; Lehtimäki, M. Electrical low pressure impactor. *J. Aerosol Sci.* **1992**, *23*, 353–360. [CrossRef]

37. Allouis, C.; Beretta, F.; Minutolo, P.; Pagliara, R.; Sirignano, M.; Sgro, L.A.; D'Anna, A. Measurements of ultrafine particles from a gas-turbine burning biofuels. *Exp. Therm. Fluid Sci.* **2010**, *34*, 258–261. [CrossRef]
38. Guyot, D.; Guethe, F.; Schuermans, B.; Lacarelle, A.; Paschereit, C. CH*/OH* Chemiluminescence Response of an Atmospheric Premixed Flame Under Varying Operating Conditions. In Proceedings of the ASME, Turbo Expo 2010: Power for Land, Sea, and Air, Glasgow, UK, 14–18 June 2010; Volume 2, pp. 933–944.
39. Kittelson, D.B.; Watts, W.F.; Johnson, J.P. On-road and laboratory evaluation of combustion aerosols—Part1: Summary of diesel engine results. *J. Aerosol Sci.* **2006**, *37*, 913–930. [CrossRef]
40. Kittelson, D.B.; Watts, W.F.; Johnson, J.P. On-road and laboratory evaluation of combustion aerosols—Part2: Summary of spark ignition engine results. *J. Aerosol Sci.* **2006**, *37*, 931–949. [CrossRef]
41. De Filippo, A.; Mariq, M.M. Diesel nucleation mode particles: Semivolatile or solid? *Environ. Sci. Technol.* **2008**, *42*, 7957–7962. [CrossRef] [PubMed]
42. Heikkilä, J.; Virtanen, A.; Rönkkö, T.; Keskinen, J.; Aakko-Saksa, P.; Murtonen, T. Nanoparticle emissions from a heavy-duty engine running on alternative diesel fuels. *Environ. Sci. Technol.* **2009**, *43*, 9501–9506. [CrossRef] [PubMed]
43. D'Anna, A. Combustion-formed nanoparticles. *Proc. Combust. Inst.* **2009**, *32*, 593–613. [CrossRef]
44. Michelsen, H.A. Probing soot formation, chemical and physical evolution, and oxidation: A review of in situ diagnostic techniques and needs. *Proc. Combust. Inst.* **2017**, *36*, 717–735. [CrossRef]
45. Commodo, M.; De Falco, G.; Bruno, A.; Borriello, C.; Minutolo, P.; D'Anna, A. Physicochemical evolution of nascent soot particles in a laminar premixed flame: From nucleation to early growth. *Combust. Flame* **2015**, *162*, 3854–3863. [CrossRef]
46. Dobbins, R.A.; Fletcher, R.A.; Chang, H.C. The evolution of soot precursor particles in a diffusion flame. *Combust. Flame* **1998**, *115*, 285–298. [CrossRef]
47. Sirignano, M.; Bartos, D.; Conturso, M.; Dunn, M.; D'Anna, A.; Masri, A.R. Detection of nanostructures and soot in laminar premixed flames. *Combust. Flame* **2017**, *176*, 299–308. [CrossRef]